

# Mode competition and output power in regular and chaotic dielectric cavity lasers

Hakan E. Türeci and A. Douglas Stone

Department of Applied Physics, P. O. Box 208284, Yale University, New Haven, CT 06520-8284

## ABSTRACT

We use the multi-mode lasing equations of Haken to analyze the stationary state lasing patterns of two-dimensional dielectric microcavity lasers of different shape, including the circle and various smooth deformations of the circle. We find a generic increase in the power output with deformation which is relatively insensitive to the specific form of the shape deformation. In addition we find strong mode selection in favor of librational modes (including but not solely the bow-tie modes) in the case when the pumping is concentrated near the center of the cavity. These results point towards an explanation of the dramatic results on power increase with deformation obtained by Gmachl et al. in quantum cascade micro-cylinder lasers. The sensitivity of the lasing solutions to the nature of the ray dynamics (chaotic, integrable and mixed) will also be analyzed.

**Keywords:** microresonators, microcavities, lasers, quantum chaos, wave chaos

## 1. INTRODUCTION

There has been a great deal of experimental and theoretical work on dielectric cavity microlasers, starting with the spherical, cylindrical and disk-shaped lasers<sup>1-3</sup> and more recently focusing on smooth deformations of these shapes, known as asymmetric resonant cavity lasers (ARCs).<sup>4-7</sup> The theoretical interest in the ARC lasers is motivated from the fact that the ray dynamics in such shapes is typically at least partially chaotic and the passive cavity represents a realization of a wave-chaotic system. The closed dielectric geometry allows a wide range of modes with different internal spatial intensity patterns and external emission patterns to have a reasonably high Q, unlike a typical Fabry-Perot cavity. This situation makes the determination of the lasing mode(s) for an ARC laser a more challenging and interesting problem. Conversely, one can regard the shape of the resonator as design parameter, which can be varied to achieve desired features in the output properties of the laser. A recent set of experiments<sup>8</sup> demonstrated very high sensitivity of the output emission pattern to variations in the resonator shape for polymer ARC cylinder lasers. This and a number of other experiments<sup>6,9-11</sup> have been interpreted in terms of specific modes of the passive ARC which can be classified as stable, unstable and chaotic. In all of these cases the lasing mode was not predicted in advance of the experiments. At least as dramatic as the shape sensitivity of the emission patterns from ARCs was the large increase in the output power of quantum cascade semiconductor ARC lasers with increasing deformation demonstrated in the experiments of Gmachl et al.<sup>6</sup> At smooth deformations from circular symmetry of 16% the lasing mode was argued to be based on a stable ray orbit with the geometry of a bow-tie; however the overall power increase with deformation was relatively smooth and for deformations of 20% was over two orders of magnitude compared to identical lasers of circular cross-section. No theory of this impressive improvement of the output power with deformation has been presented up to this point.

The difficulty in the theory is that consideration of the passive cavity is clearly insufficient to explain the phenomena. The passive cavity can give us insight into the relative Q-values of the modes and their emission patterns; however only a non-linear theory which includes many modes and their competition can address the mode selection and output power of these lasers. In particular, the circular (cylindrical) laser cavities will have individual modes with approximately the same Q-values as the bow-tie modes believed to be responsible for the lasing output at high deformations in the experiments of Gmachl et al.<sup>6</sup> However clearly the mode competition and spatial distributions of the modes should be different in the two cases and must be responsible for the vastly different output properties.

In this manuscript, we will study the interacting mode problem for 10-100 micron-scale lasers based on dielectric resonators, both cylindrical and deformed cylinders (ARCs). To do this one needs to study a non-linear

lasing theory with many modes interacting. We start with the *semi-classical laser theory*, developed by Haken,<sup>12</sup> Lamb<sup>13</sup> and others, which leads to the coupled non-linear Maxwell-Bloch equations. An approximate multi-mode treatment of these equations, valid near threshold, was developed by Haken and Sauermann<sup>14</sup> and is used below in this new context to address the output power and selection of the lasing modes in such systems. This model has the virtue of allowing the simultaneous treatment of a large number of modes, consistent with the number of modes relevant to lasing in the experimental systems of interest. The drawback of the model is that it likely overestimates the number of lasing modes, due to the near threshold approximation (we will comment on this further below). However it is currently not possible to improve this approximation and still include the number of modes required for treatment of the realistic system. In this regard, we note that there have been a number of interesting recent papers by Harayama and coworkers<sup>15-17</sup> on the theory of such lasers working with the full Maxwell-Bloch equations or a slightly simplified (so-called Schrödinger-Bloch) version. These papers address a number of issues as to possible lasing modes and mode-locking effects which we shall also discuss below; however they do not address mode selection, shape sensitivity and power output in the many mode regime as we do in the current work. Our results suggest that both the overall decrease in Q-values with deformation and spatial selective pumping effects account for the power increase observed in the experiments of Gmachl et al. In addition, the output emission pattern observed in that experiment reflects the importance of mode-locking of quasi-degenerate bow-tie modes, in a similar manner to the recent observation of Fukushima et al.<sup>16</sup>

## 2. DERIVATION OF MULTI-MODE EQUATIONS FROM THE MAXWELL-BLOCH EQUATIONS

The starting point for our theoretical treatment is the following form of the Maxwell-Bloch (MB) equations:

$$\dot{e} = \frac{i}{2\omega_a} [\omega_a^2 + c^2\nabla^2] e + 2i\pi\omega_a p \quad (1)$$

$$\dot{p} = -\gamma_{\perp} p + \frac{g^2}{i\hbar} e D \quad (2)$$

$$\dot{D} = \gamma_{\parallel} (D_0 - D) - \frac{2}{i\hbar} (ep^* - pe^*) \quad (3)$$

This is a set of non-linearly coupled spatio-temporal partial differential equations for the field amplitudes  $e(x, y, t)$ ,  $p(x, y, t)$  and the inversion  $D(x, y, t)$ . The full electric and polarization field are given by  $E(x, y, t) = e(x, y, t)e^{-i\omega_a t} + c.c.$  and  $P(x, y, t) = p(x, y, t)e^{-i\omega_a t} + c.c.$ . Here we have concentrated on the  $k_z = 0$  TM modes of the electric field with polarization in the  $z$ -direction (along the axis of the cylinder). Hence there is no  $z$ -variation (neglecting edge effects at top and bottom) and the fields are functions of the transverse coordinates  $\mathbf{x} = (x, y)$  making the problem effectively two-dimensional. The parameters  $\omega_a$  and  $g$  are the atomic transition frequency and the dipole moment matrix element, while  $\gamma_{\perp}$  and  $\gamma_{\parallel}$  are phenomenological damping constants for the polarization and the inversion, respectively. Note that field damping is implicit in the operator  $\mathcal{L} = \frac{i}{2\omega_a} [\omega_a^2 + c^2(\partial_x^2 + \partial_y^2)]$  which in this way will provide us with mode-dependent cavity decay rates  $\kappa_{\mu}$ , contrary to the conventional models with a fixed, heuristic  $\kappa$ .

We will focus on semiconductor lasers (Class B)<sup>18</sup> for which we can adiabatically eliminate the polarization, i.e.  $\dot{p} = 0$  and

$$p(\mathbf{x}, t) = \frac{g^2}{i\hbar\gamma_{\perp}} e(\mathbf{x}, t) D(\mathbf{x}, t) \quad (4)$$

In this case the adiabatic elimination is well-justified as for typical semiconductor lasers  $\gamma_{\perp}$  is at least three orders of magnitude larger than the other time scales  $\kappa$  and  $\gamma_{\parallel}$ .

A multi-frequency solution<sup>19</sup> is only possible when the inversion is stationary  $D(\mathbf{x}, t) = D(\mathbf{x})$ , so that  $\dot{D} = 0$  also. A stationary multi-mode solution can be found when the typical mode spacing  $\Delta \gg \gamma_{\parallel}$  so that time-dependent (beating) terms in  $D(\mathbf{x}, t)$  are reduced by the factor  $\gamma_{\parallel}/\Delta$ . The typical mode spacing for a roughly circular cavity scales as  $\Delta \sim c/kR^2$ , where  $R$  is the average radius of the cavity; as is well-known, closely-spaced modes of the cold cavity may frequency-lock in the active cavity. Due to the discrete symmetries of the cavities we consider (such as reflection) there are guaranteed to be quasi-degenerate multiplets from stable orbit

modes<sup>20</sup> which in the cold cavity would violate our assumption that the mode spacing is much greater than  $\gamma_{\parallel}$ ; however we will assume that such modes frequency-lock and the resulting modes are then well-separated and treatable within our adiabatic approximation. We will discuss the effect of this frequency-locking in more detail in Section 5 below; for the moment we include this effect by allowing the possibility of two different cold-cavity modes having the same frequency. Implementing  $\dot{D} = 0$  gives

$$D(\mathbf{x}) = \frac{D_0}{1 + \frac{4g^2}{\hbar^2 \gamma_{\perp} \gamma_{\parallel}} |e(\mathbf{x})|^2} \quad (5)$$

We now introduce expansions of the fields in the cold-cavity modes  $\psi_{\mu}(\mathbf{x})$ , which we assume to be real:

$$e(\mathbf{x}) = \sum_{\mu} e_{\mu}(t) \psi_{\mu}(\mathbf{x}), \quad p(\mathbf{x}, t) = \sum_{\mu} p_{\mu}(t) \psi_{\mu}(\mathbf{x}) \quad (6)$$

where  $e_{\mu}(t) = e_{\mu}^{(0)} e^{i\Omega_{\mu} t}$  and we do not assume that the lasing frequencies  $\Omega_{\mu}$  are given by the cold-cavity frequencies. It is conventional in this approach to take the cold cavity modes as the solutions of the ideal *closed* cavity, which have real frequencies and are orthogonal. In the results given below we will follow this approach and use approximate arguments to estimate the transmissivity and lifetimes of the corresponding modes of the open dielectric cavity. We are developing an improved treatment in which the modal expansion is in terms of linear amplifying states, which are solutions of the wave equation for piecewise constant (in space) complex (amplifying) index of refraction with real  $k$ , and satisfy somewhat more complicated orthogonality relations.

Rewriting Eq. (5) and neglecting terms of lower order after time-averaging over fast motion

$$D(\mathbf{x}) = \frac{D_0}{1 + \frac{1}{e_c^2} \sum_m e_m \sum_{\bar{m}} e_{\bar{m}} \psi_m(\mathbf{x}) \psi_{\bar{m}}(\mathbf{x})} \quad (7)$$

where the sum on  $m$  runs over all lasing modes but the sum on  $\bar{m}$  runs just over any frequency-locked cold cavity modes corresponding to  $m$ . Here,  $e_c = \frac{\hbar \sqrt{\gamma_{\parallel} \gamma_{\perp}}}{2g}$ , the typical electric field scale above the laser threshold (after the exponential growth). Note that the inclusion of retardation effects for the polarization degree of freedom could be taken into account by replacing  $e_c$  by a mode-dependent  $e_{c\mu}^{-2} = \frac{4g^2 \gamma_{\perp}}{\hbar^2 \gamma_{\parallel}} \frac{1}{\Omega_{\mu}^2 + \gamma_{\perp}^2}$ , although we will not do this here.

Plugging Eq. (7) into Eq. (1), using Eq. (6) and spatially integrating both sides of the equation against  $\psi_{\mu}(\mathbf{x})$ , (using the orthogonality of the modes) we obtain

$$\dot{e}_{\mu} = (i\tilde{\Delta}_{\mu} - \tilde{\kappa}_{\mu})e_{\mu} + \sum_{\nu} D_{\mu\nu} e_{\nu} \quad (8)$$

Here, we have scaled the time and all frequencies with respect to a typical cavity decay scale  $\kappa$  (this could be the cavity decay rate of the shortest lifetime mode in a given spectral interval within the linewidth of the laser). The symmetric inversion matrix  $D_{\mu\nu}$  is given by

$$D_{\mu\nu} = \tilde{D}_0 \int d^2x \frac{\psi_{\mu}(\mathbf{x}) \psi_{\nu}(\mathbf{x})}{1 + \frac{1}{e_c^2} \sum_{m, \bar{m}} e_m e_{\bar{m}}^* \psi_m(\mathbf{x}) \psi_{\bar{m}}(\mathbf{x})} \quad (9)$$

Here  $\tilde{D}_0 = D_0/D_c$ , where  $D_c = \frac{\hbar \kappa \gamma_{\perp}}{2\pi \omega_a g^2}$  is the single mode pump threshold corresponding to a chosen reference mode with lifetime  $\kappa$ . It is here that we make the key near-threshold approximation and expand the denominator of Eq. (7) to give

$$\dot{e}_{\mu} = (i\tilde{\Delta}_{\mu} - \tilde{\kappa}_{\mu} + \tilde{D}_0)e_{\mu} - \tilde{D}_0 \sum_{m\bar{m}\nu} e_{\nu} e_m e_{\bar{m}}^* \Gamma_{\mu m \bar{m} \nu}. \quad (10)$$

The expansion is valid as long as our pump satisfies  $|D_0 - D_c| \ll D_c$ . Here,

$$\Gamma_{\mu m \bar{m} \nu} = \int d^2x \psi_{\mu}(\mathbf{x}) \psi_m(\mathbf{x}) \psi_{\bar{m}}(\mathbf{x}) \psi_{\nu}(\mathbf{x}) \quad (11)$$

The usual approximation to this third order theory would neglect the possibility of mode-locked cold cavity states and set  $\bar{m} = m$ ; we shall refer to this as the *diagonal theory*. Then, multiplying both sides of Eq. (10) by  $e_\mu^*$  and time-averaging the product  $e_\mu^* e_\nu$  we obtain:

$$\frac{1}{2}\dot{n}_\mu = -(\kappa_\mu - D_0)n_\mu - D_0 \sum_\nu A_{\mu\nu} n_\nu n_\mu \quad (12)$$

Here  $n_\mu = |e_\mu|^2$  are the modal intensities, we have dropped the tilde for the scaled quantities, relabeled the index  $m \rightarrow \nu$  and  $A_{\mu\nu}$  are the overlap integrals

$$A_{\mu\nu} = \Gamma_{\mu\nu\mu\nu} = \int d^2x \psi_\mu^2(\mathbf{x}) \psi_\nu^2(\mathbf{x}). \quad (13)$$

### 3. RESULTS OF DIAGONAL THEORY

Setting  $\dot{n}_\mu = 0$ , the steady state solution of Eq. (12) yields

$$1 - \frac{\kappa_\mu}{D_0} = \sum_\nu A_{\mu\nu} n_\nu \quad (14)$$

Therefore the near threshold modal intensities are determined by solving an inhomogeneous linear system determined by the overlap matrix,  $A_{\mu\nu}$  (which encodes both the mode volume effects in the diagonal terms and the spatial hole-burning effects in the off-diagonal terms), the lifetimes of the cold cavity modes  $\kappa_\mu$ , and the pump power  $D_0$ . However there is an important constraint on this equation which prevents a straightforward inversion: all physical solutions require  $n_\mu > 0$ . The technique we use to implement the constraints is described below. Our results on power output below will all be based on the solution of this set of near threshold equations for various resonators.

As just noted, a physical solution requires all  $n_\mu > 0$ . It is possible to satisfy this constraint by varying the number of modes included; above the lowest lasing threshold one is guaranteed that at least one solution exists with some  $n_\mu \neq 0$  and all others zero. Typically one finds solutions with tens of modes lasing in the parameter region we investigate. However Eq. (14) does not have a unique solution using this approach for a given pump strength. The solution depends strongly on the set of included modes  $\{\psi_\mu\}$ . Only one of these solutions represents a stable solution at a given pump value  $D_0$ , all the other solutions being unstable. We find this stable solution in the following way: One starts with the mode  $\psi_0$  which has the lowest threshold and determines the instability threshold of the next mode by finding the lowest value of  $D_0$  at which inclusion of the mode  $\{\psi_\mu\}$ ,  $\mu \neq 0$  yields a positive solution. This is then iterated by including more and more modes.

#### 3.1. Circular resonators

We first consider circular resonators; the non-linear modes of such resonators have been studied previously by Harayama et al.<sup>21</sup> For this problem each mode is exactly degenerate, corresponding to angular variations  $\cos m\phi$  and  $\sin m\phi$ , and as we will show below, in the non-linear regime these modes combine (lock) with a phase difference of  $\pi/2$ . Hence the basis set of cold-cavity modes we will use have an angular variation of  $e^{\pm im\phi}$ . For the circular dielectric cavities we have a very accurate analytical approximation for the lifetimes  $\kappa_\mu$  using the semiclassical interpolation formula<sup>22</sup>

$$\kappa_\mu = \frac{1}{2} \log \left[ \frac{n-1}{n+1} \right] \frac{J_m(kR)Y_{m-1}(kR) - J_{m-1}(kR)Y_m(kR)}{J_m^2(kR) + Y_m^2(kR)}. \quad (15)$$

To obtain the output intensity, we will multiply the modal intensities  $n_\mu$  obtained from the solution of Eq. (14) by the associated semiclassical transmissivity  $T_\mu = 4\kappa_\mu \cos \chi_\mu$ ,<sup>22</sup> where we use the WKB value for  $\sin \chi_\mu = m/nk_\mu R$ .

The calculated overlap matrices  $A_{\mu\nu}$  are shown in Fig. 1. Note that the diagonal elements are the inverse mode volumes; along with the lifetimes, they determine the internal/external intensities in the single-mode theory. The mode volumes are lowest for the extreme whispering gallery modes and are largest for values of

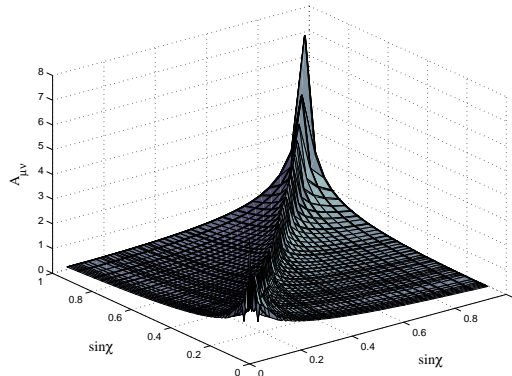


**Figure 1.** The overlap matrix  $A_{\mu\nu}$ . The modes are ordered such that  $\sin \chi$  increases monotonically with  $\sin \chi \approx 1$  corresponding to whispering gallery modes and  $\sin \chi \approx 0$  corresponds to bouncing ball (Fabry-Perot) modes

$\sin \chi \sim 0.4$ ; they decrease again for bouncing ball type modes which pass through the center of the resonator. The off-diagonal elements are typically 2-8 times less than the diagonal elements and decrease away from the diagonal since modal interactions are strongest for spatially overlapping modes.

The stable solution for input and output modal intensities to Eq. (14) for the input data given in Fig. 1 is plotted in Fig. 2 for  $D_0 = 1.1$ . The internal modal intensities are controlled by mode volume effects with a maximum away from the critical angle for total internal reflection; however the external modal intensities are modified strongly by the escape probabilities, so that very intense whispering gallery modes give little external intensity while leakier modes nearer the critical angle give the largest contribution. This demonstrates the necessity of having an optimal Q value to provide efficient output and the selection of such modes in the circle.

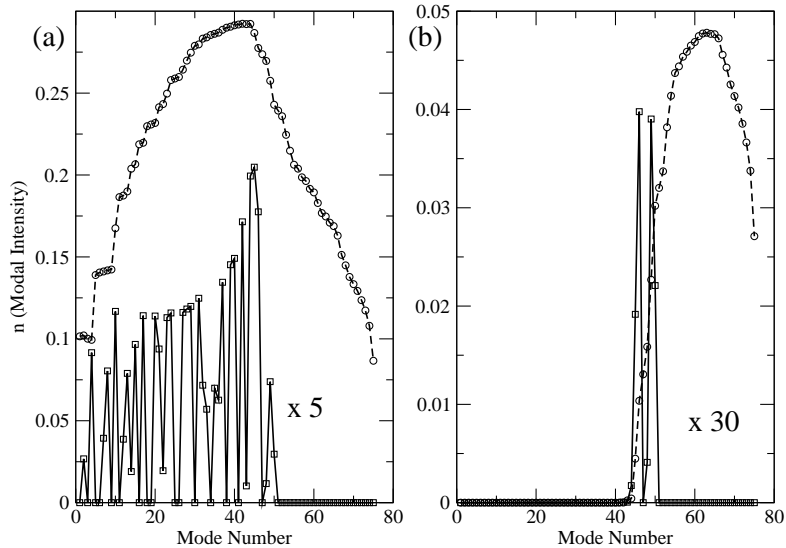


**Figure 2.** (a) Internal and (b) external modal intensities (in units of  $e_c$ ) calculated within the single-mode theory compared to the model with modal interactions Eq. (14) for  $D_0 = 1.1$  and an absorption of  $\kappa_0 = 0.3$ . The gain center is at  $nkR \approx 128$  and the linear index of refraction of the cavity is  $n = 3.3$ . The last mode lasing corresponds to a mode with an angle of incidence given by  $\sin \chi = 0.2785$ , which is a classically emitting mode below the critical angle  $\sin \chi_c = 0.3030$ . The interacting modal intensities are much smaller than the non-interacting (single-mode) intensities and have been scaled by a factor of 5 for the internal, and by a factor of 30 for the external case to expedite the comparison

The thresholds within the interacting mode model are strongly modified with respect to their single-mode values, as can be seen from Fig. 3.

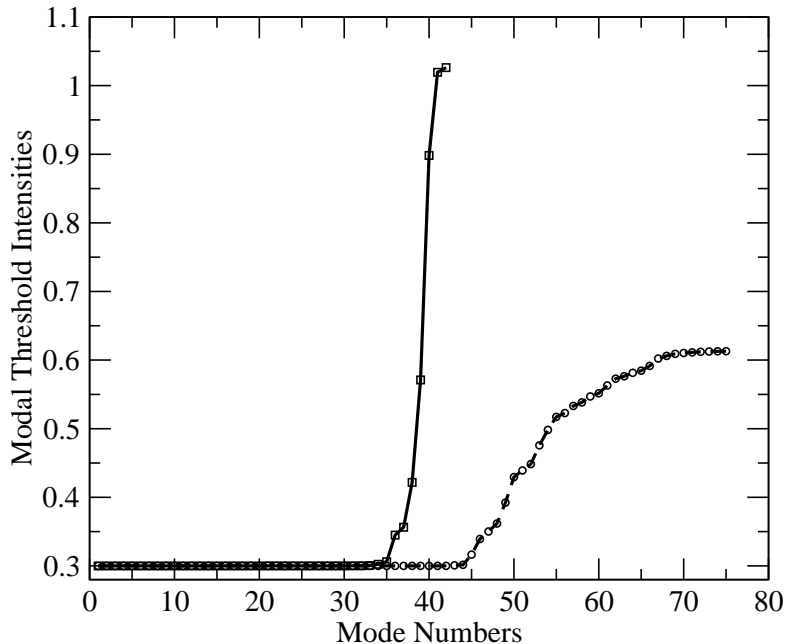


**Figure 3.** Interacting (squares) and single-mode (circles) threshold pump intensities upto a maximum pump power of  $D_0 = 1.1$ .

In Fig. 4 we study the effect of mode interactions on the output modal intensities. We plot the *ratio* of the maximum output modal intensities obtained from the single-mode (neglecting interactions) theory to that with interaction included. In all cases turning on interactions suppresses somewhat the intensity, but only by a factor of roughly three for the internal intensity, whereas it can suppress the external intensity by factors of as much as thirty. Moreover the output intensity is highly sensitive to the value of the pump, whereas the internal intensity is not. This indicates that for the circular lasers we can get a much lower output intensity than what we would expect from the lifetime of a given mode based on single-mode considerations.

As already noted, our near threshold theory cannot give us a completely realistic description of experiments, where saturation effects play a role. The near threshold theory actually underestimates the modal intensities for a given mode which is well above threshold. An indication of this comes from the single-mode approximation, for which one can directly compare near threshold and saturated expressions for the modal intensities. In this analysis it is important to include the linear absorption loss within the resonator.

The saturated expression for external modal intensities is given by

$$n_{\mu}^{out} = 4\kappa_{\mu} \cos \chi_{\mu} \left( \frac{D_0}{\kappa_0 + \kappa_{\mu}} - 1 \right) \quad (16)$$

Here,  $\kappa_0$  is the linear absorption rate. We will compare this expression to our near-threshold form

$$n_{\mu}^{out} = 4\kappa_{\mu} \cos \chi_{\mu} \left( 1 - \frac{\kappa_0 + \kappa_{\mu}}{D_0} \right) \quad (17)$$

Note that the threshold condition is identical in both expressions, however the behavior well above threshold is very different. The near threshold form will lead to a saturation of the modal intensities with pump strength at a dimensionless value of unity, whereas the general expression leads to a linear increase in modal intensities for high pump strength. Thus the modal intensities are underestimated for the higher Q modes within the near threshold theory, leading to an underestimate of the power output. This error is smaller the larger is the linear absorption coefficient, which brings down the Q values of whispering gallery modes; thus the near threshold theory improves with larger linear absorption at a given value of the pump, as shown in In Fig. 5. This underestimate of the

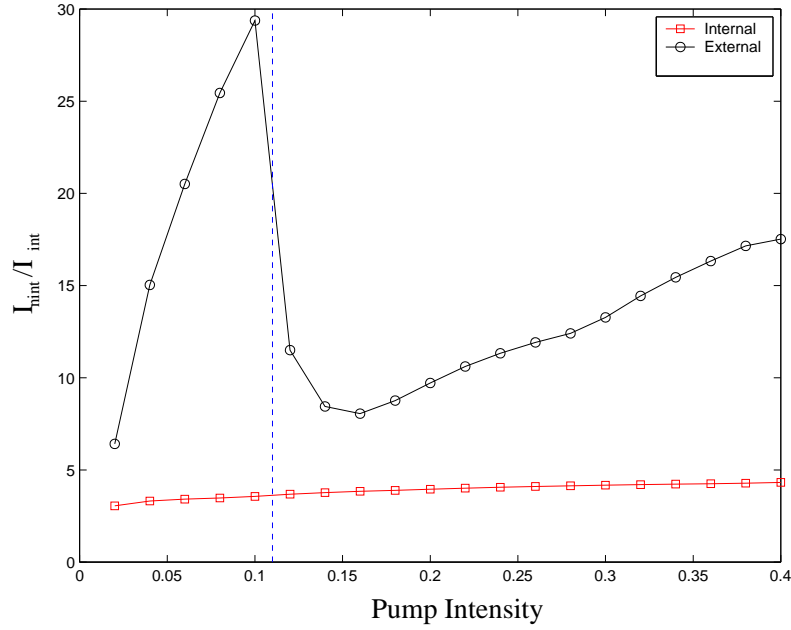


**Figure 4.** The ratio of the non-interacting and the interacting maximum modal intensities as a function of the pumping power  $D_0$ . Squares are the internal modal intensities, while the circles represent the output modal intensities collected in the farfield.

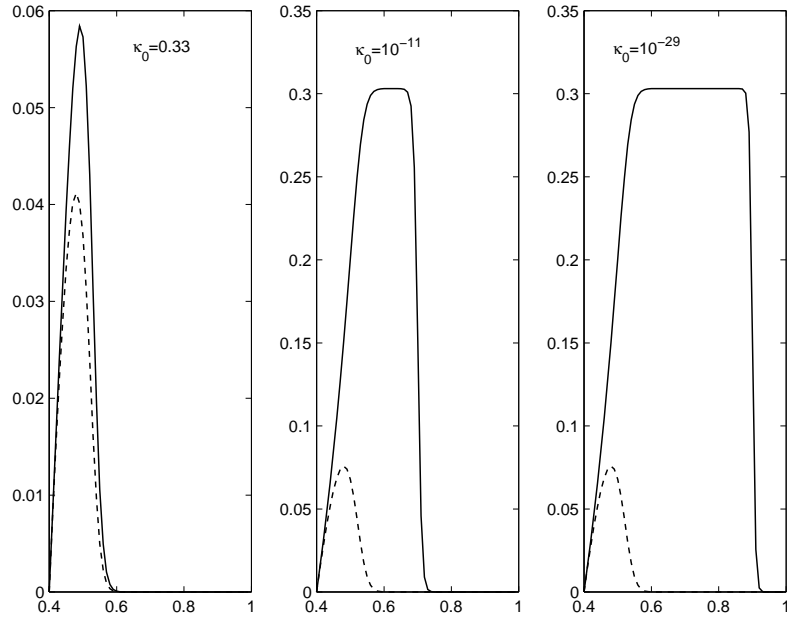


**Figure 5.** Variation of the output modal intensities with respect to their semiclassical incidence angle  $\sin \chi$  for the expression with saturation (solid) and without saturation (dashed). Here, the pump  $D_0$  is such that the mode with  $\sin \chi = 0.46$  is at the threshold i.e. it's varying with  $\kappa_0$ .

modal intensities makes quantitative comparison with experiments difficult; nonetheless it allows qualitative conclusions. When modal interactions are included, we no longer can compare the near threshold theory to a more exact result, however we expect the effect of mode competition to be even greater in the exact theory. The larger intensities of the modes which are already lasing prevents modes with large spatial overlap (and similar lifetime) from lasing to an even greater degree than we find in our near threshold theory. This likely accounts for

the larger number of lasing modes our theory finds in both the circular and deformed resonators in comparison to experiments.

#### 4. DEFORMED CYLINDRICAL RESONATORS AND POWER OUTPUT

Having established that mode competition plays a major role in suppressing power output from circular resonators we now analyze deformed cylinders (ARCs) of both elliptical and quadrupolar shapes. The elliptical deformations, defined by  $r(\phi) = R_0/(1 + [(1 + \epsilon)^4 - 1] \sin^2 \phi)$ , are special because they are known to induce no chaos in the ray dynamics. In contrast, the quadrupolar deformation, defined by  $r(\phi) = R_0(1 + \epsilon \cos 2\phi)$ , induces ray chaos for a large fraction of the phase space for deformations above roughly 20 % major to minor axis ratio ( $\epsilon \geq 0.10$ ) (see Fig. 6). Nonetheless the quadrupolar shape in this deformation range does have one stable short periodic orbit (other than the two-bounce Fabry-Perot motion, which does not provide high-Q resonances); that is the bow-tie orbit (see Fig. 6(B)) mentioned above as the mode which appears to be the dominant lasing mode in the experiments of Gmachl et al.<sup>6</sup> It is the huge power increase which deformation, as well as the selection of the bow-tie mode, which we hope to explain with our theory.

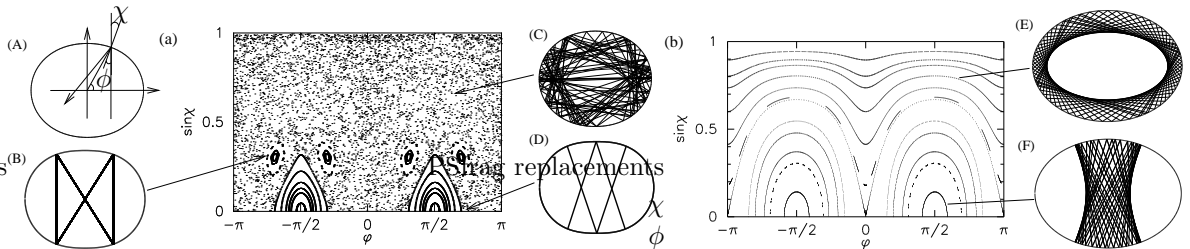


**Figure 6.** Surface of section for (a) a quadrupole and (b) an ellipse at deformation  $\epsilon = 0.16$  obtained for 30 different trajectories iterated for 600 reflections. (A) The coordinate system used, (B) the stable “bowtie” orbit, (C) a chaotic orbit, (D) the unstable “bird” orbit, (E) a quasi-periodic whispering gallery orbit and (F) a quasi-periodic bouncing-ball type orbit.

It should however be noted that while the emission from the “bow-tie” lasers becomes highly directional and consistent with a bow-tie mode at deformations around  $\epsilon = 0.16$ , the power output increase with deformation is found to be smooth and does not show a sharp spike at the deformation at which the emission pattern suggests that the bow-tie mode is “turning on”. It therefore is likely that the power increase is a more general phenomenon, not associated specifically with the bow-tie modes. Moreover the resonator shape for Gmachl et al. was not an exact quadrupole but was actually somewhat flatter, suggesting that the exact shape is not crucial.

##### 4.1. Deformation and uniform pumping

We calculated the cold-cavity modes for a range of quadrupolar and elliptical shapes covering roughly the range measured experimentally, constructed the overlap matrices  $A_{\mu\nu}$  and then solved the constrained linear system of equations Eq. (14) in the manner already described. This yielded the internal and external lasing spectrum for a given shape and by summation over modes, the power output from that shape.

In Fig. 7 we show the power output vs. deformation for both the quadrupolar and elliptical deformations. We find that both the ellipse and the quadrupole exhibit roughly a factor of four increase in power with deformation up to the value of  $\epsilon = 0.16$  indicating an effect which does not depend sensitively on the type of shape deformation. As noted above, our near threshold theory likely underestimates the power output one expects in a theory with saturation, therefore the factor of four increase found is still significant.

In Fig. 8 we analyze the external lasing spectrum for the quadrupole with  $\epsilon = 0.16$ . Many modes again are lasing as in the circular case and there seems to be no strong selection of particular mode geometries. In particular there is no evidence of strong selection of bow-tie or other similar (librational) modes. In order to determine the origin of the power increase with deformation in this case of uniform pumping we tried to separate out the change in the mode competition with deformation (off-diagonal elements of  $A_{\mu\nu}$ ) from the lifetime effects ( $\kappa_\mu$ ). To this end we defined an overlap matrix based on the assumption of Gaussian random modes,

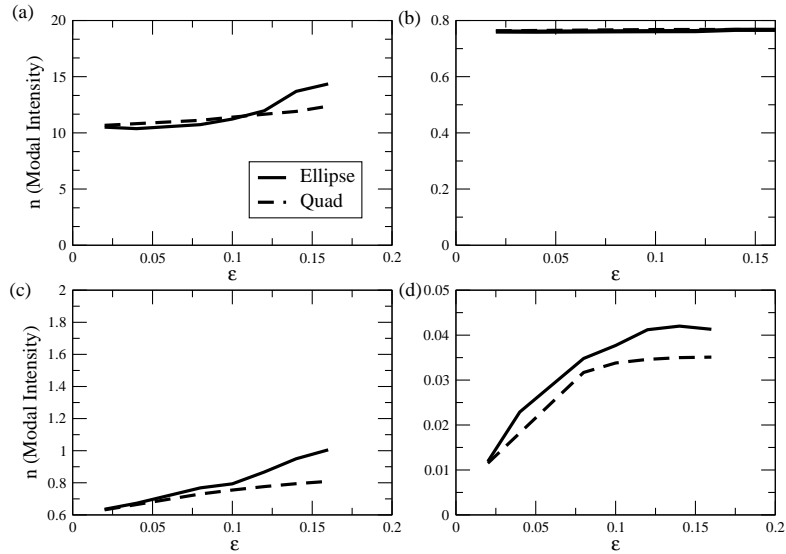


**Figure 7.** The total internal modal intensities with respect to deformation for the case of (a) non-interacting (single-mode theory) and (b) interacting modes. In the lower panel, we plot the total external modal intensities with respect to deformation for the case of (c) non-interacting (single-mode theory) and (d) interacting modes. The calculations were performed at a constant pump strength  $D_0 = 0.9$  and a linear absorption  $\kappa_0 = 0.1$ .

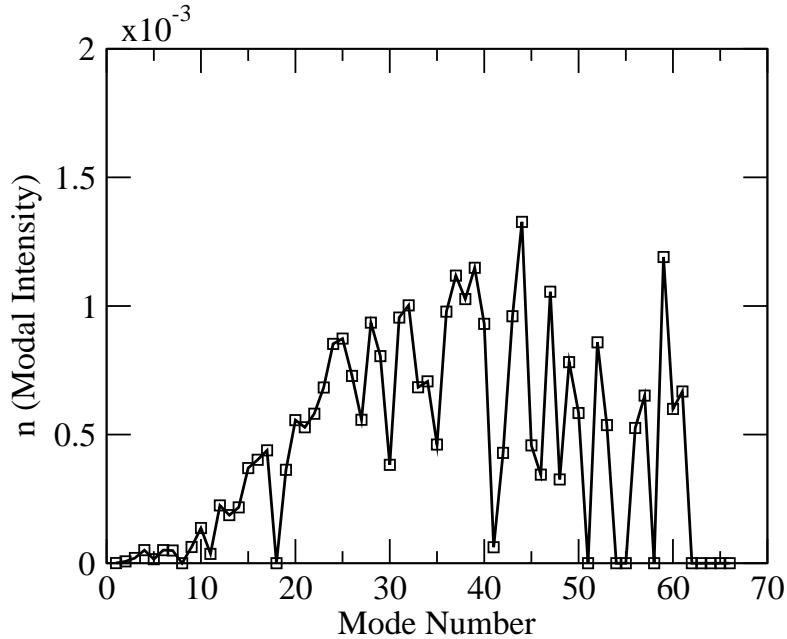


**Figure 8.** Output modal intensities for a quadrupolar cavity of  $\epsilon = 0.16$  and a linear index of refraction  $n = 3.3$ . The gain center is at  $nkR = 128$ , the pump strength is  $D_0 = 0.9$  and the absorption rate is  $\kappa_0 = 0.1$ .

as one would get for a system described by random matrix theory.<sup>23</sup> Once self-averaging effects are included this matrix has just constant off-diagonal elements for all pairs of modes, implying a constant level of mode competition:

$$A_{\mu\nu} = 1 + 2\delta_{\mu\nu} \quad (18)$$

We combined this overlap matrix with the cavity decay rate distributions appropriate for the ellipse and quadrupole of various deformations. The results for the elliptic lifetimes are shown in Fig. 9; those for the

quadrupole were similar. We found that with this constant off-diagonal matrix the total power output increased even more dramatically with deformation, by roughly a factor of 30, indicating that lifetime effects dominate the power increase in this case. For the deformed shapes more of the lasing modes are strongly emitting, leading to an increase in power output with deformation.

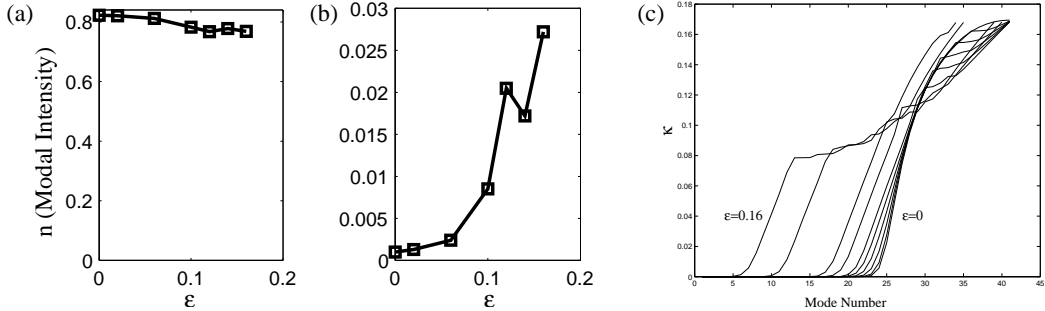


**Figure 9.** Variation of (a) Internal and (b) external modal intensities with the elliptic deformation parameter  $\epsilon$  calculated for the constant interaction model Eq. (18) and lifetime distributions obtained from the elliptic cavity with the corresponding deformation. (c) A plot of the cavity decay rate ( $\kappa$ ) for the elliptic cavity with varying deformation  $\epsilon$  vs. mode number (ordered from lowest to highest decay rate). The fraction of highly emitting modes increases substantially with increasing deformation of the ellipse.

## 4.2. Deformation and selective pumping

The failure of the uniform pumping theory to show any tendency to select bow-tie or similar modes as one might have expected from the experiments motivated us to conjecture that the experiments do not correspond to the uniform pumping scenario. In fact in the experiments the current is injected near the axis of the cylinder by a needle contact and a current spreading layer is fabricated to allow the current to become more uniform across the cross-section by the time it reaches the active layers. There is no doubt that there is at least somewhat higher current in the center than at the edges and this would favor modes with high intensity in the center of the resonator. For the circular cylinders the only such modes are those Fabry-Perot modes with normal incidence and low Q. In both the ellipse and the quadrupole, as the cross-section is deformed new modes appear which correspond to ray orbits which cross the center of the resonator but impact the boundary at a steep enough angle to be well-confined and hence to have much higher Q. The most prominent of these modes is the bow-tie in the quadrupole (although there are others like it) and there are families of similar oblique-incidence librational orbits in the ellipse. It is therefore plausible that selective pumping of the central region would be much more efficient at pumping the deformed shapes than the circular cylinders and that it would not matter too much whether the deformation was quadrupolar or elliptical.

In Fig. 10 we show the external modal intensities for the quadrupolar deformation of  $\epsilon = 0.16$  within the same theory, but with selective pumping described by a rotationally-symmetric Gaussian pump profile  $D_0(\mathbf{x}) = D_0 \exp(-|x|^2/a^2)$  in space. The spatial non-uniformity of pumping can be easily taken into account in the near-threshold formalism; Eq. (14) is modified to

$$B_{\mu\mu} - \frac{\kappa_{\mu}}{D_0} = \sum_{\nu} A_{\mu\nu} n_{\nu} \quad (19)$$

where  $B_{\mu\mu} = \int d^2x D_0(\mathbf{x}) \psi_{\mu}(\mathbf{x}) \psi_{\mu}(\mathbf{x})$  and  $A_{\mu\nu} = \int d^2x D_0(\mathbf{x}) \psi_{\mu}^2(\mathbf{x}) \psi_{\nu}^2(\mathbf{x})$  to accommodate the position dependence of the pump. With such a selective pumping one finds that the lasing intensities do not vary smoothly with the single-mode thresholds (our ordering of the mode numbers), but instead a small number of modes are strongly preferred. When the spatial patterns of the preferred modes are analyzed they are found to be all of the librational type, with bow-tie modes dominating and a large contribution from the specific second-order bow-tie modes believed to be observed in the experiments of Gmachl et al.<sup>6</sup> (see figure caption and discussion in Section 5.1.2 below). Thus we conjecture that spatially selective pumping plays a key role in the selection of bow-tie

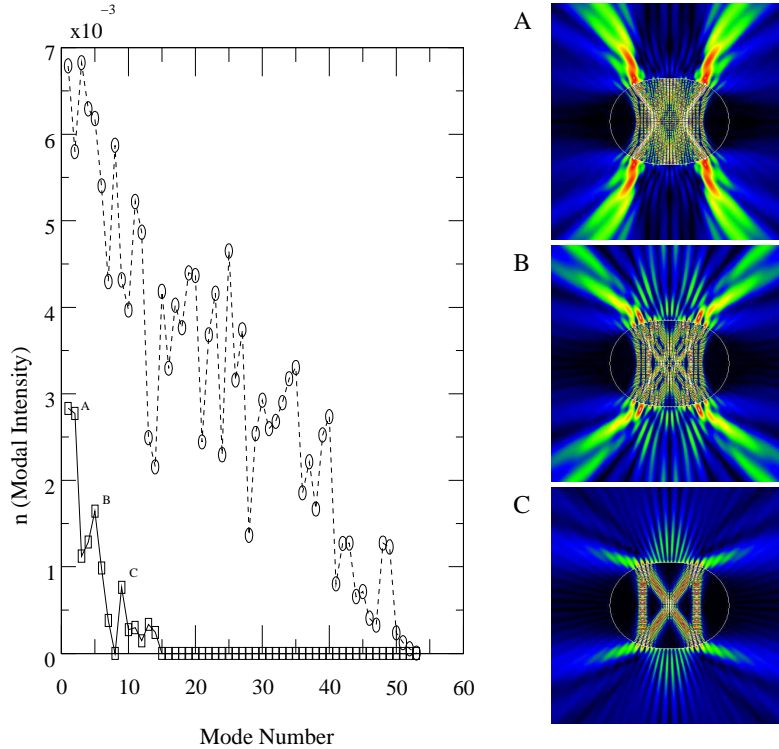


**Figure 10.** Output modal intensities for a quadrupolar cavity of  $\epsilon = 0.16$  and a linear index of refraction  $n = 3.3$ . The gain center is at  $nkR = 128$ , the pump strength is  $D_0 = 1.0$  and the absorption rate is  $\kappa_0 = 0.3$ . The squares represent interacting modes, while circles are the data for non-interacting modes. The pumping profile was chosen to be of a Gaussian profile with a standard deviation of  $a/R_0 = 0.7$ . The inset shows the spatial structure of some of the lasing modes: (A) A scarred state based on the “bird” orbit, (B) the second order transverse mode corresponding to the stable “bowtie” orbit and (C) the ground-state bowtie mode. The sudden onset of directional emission at a  $45^\circ$  angle to the symmetry axes in the experiments of Gmachl et al.<sup>6</sup> was interpreted as due to the second order bow-tie although the peak location is consistent with emission from the “bird” modes as well.

modes in that experiment, but may not be crucial for obtaining a large power increase with deformation. Again these conclusions appear not to depend strongly on whether the resonator shape is quadrupolar or elliptical.

In Fig. 11 we plot the power increase vs. deformation for the two shapes and find them to be almost identical and both in the range of a factor of five. While we believe our theory gives the right trends and qualitative features, we do not expect this near-threshold theory to explain the two order of magnitude effect seen in the experiments. One clear indication of the need for further refinement of the theory is the large number of lasing modes we find, whereas the experiments found<sup>6</sup> only four or five lasing modes above the noise level, and all of these appeared to be second order (two transverse nodes) bow-tie modes. Our calculations for the quadrupole finds not only second order bow-tie modes, but first order and ground state modes lasing strongly as well as other librational modes. It is likely that the specific dominant mode among similar types is quite sensitive to shape; this is something which requires further study. However as noted above, our near threshold theory likely produces many more lasing modes than a full theory with saturation would do; so while the theory can be used to determine the general type of lasing mode selected, it is not able to predict the specific lasing mode.

In conclusion, the power increase with deformation of these dielectric cylinder resonators is a robust and generic effect which is related to improved output coupling with deformation; this effect can be enhanced by selective pumping of the central region of the cylinder, which will also select for librational modes which have high intensity at the center but scatter off the boundary with a high enough angle of incidence to be near the critical angle for total internal reflection. The effect does not seem to be very sensitive to the nature of the ray dynamics of the shape and specifically to whether these dynamics are integrable or primarily chaotic. However

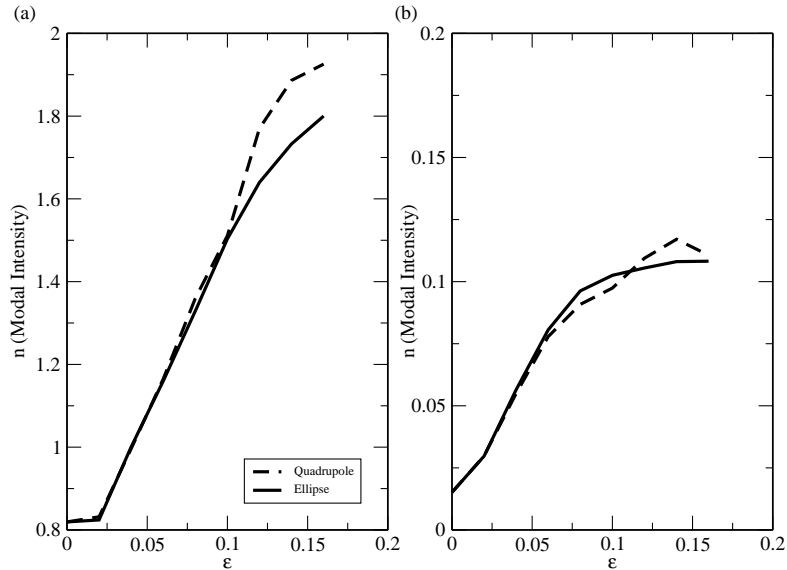


**Figure 11.** The total external modal intensities with respect to deformation for the case of (a) non-interacting (single-mode theory) and (b) interacting modes for elliptical and quadrupolar deformations. The interacting case shows a factor of five increase of output power with deformation and no significant difference between elliptical and quadrupolar deformations. The calculations were performed at a constant pump strength  $D_0 = 0.9$  with selective pumping defined by  $a/R_0 = 0.7$  and a linear absorption  $\kappa_0 = 0.1$ .

the effect of shape on the lasing properties and on the emission patterns requires more detailed study before firm conclusions can be reached.

## 5. OFF-DIAGONAL THEORY AND MODE-LOCKING

For resonators which have discrete symmetries such as reflection or inversion, multiplets of nearly degenerate modes are unavoidable as long as there exist modes localized on periodic orbits (such as the bow-tie modes just discussed). The symmetries will lead to multiple orbits related by symmetry and to quasi-degenerate modes associated with these orbits. Even if the system has no symmetry, any orbit which does not retrace itself will have a time-reversed partner leading to degenerate or quasi-degenerate pairs of modes (exact degeneracy only occurs for the circle). Since the splitting of these multiplets are typically exponentially small they are subject to mode-locking (cooperative frequency locking) in the non-linear theory. Thus our multi-mode formulation of the theory must be generalized to take into account this mode-locking behavior as well as competition of such modes.

Starting with Eq. (10) we will specialize to the case of mode-locked doublets as we would have e.g. in the circle, or for bow-tie modes in the quadrupole. We will describe the interaction of such locked doublets, where each linear mode of the doublet denoted by  $\mu$  locks (i.e. has the same frequency) to their partners  $\bar{\mu}$ , but there are many such pairs well-separated in frequency as for a sequence of bow-tie modes corresponding to different longitudinal node number. The stationary inversion can be written as

$$D(\mathbf{x}) = \frac{D_0}{1 + \frac{1}{e_c^2} \left( \sum_{\mu} |e_{\mu}|^2 \psi_{\mu}^2 + \sum_{\mu\bar{\mu}} e_{\mu} e_{\bar{\mu}}^* \psi_{\mu} \psi_{\bar{\mu}} \right)} \quad (20)$$

Here,  $\mu \neq \bar{\mu}$ . Writing  $e_{\mu} = \sqrt{n_{\mu}} e^{i\phi_{\mu}}$ , multiplying both sides of Eq. (10) with  $e_{\mu}^*$ , subtracting from the equation for  $e_{\bar{\mu}}$  and performing a time-average over an interval  $\tau \gg \Delta^{-1}$ , we obtain

$$\frac{1}{2}\dot{n}_\mu = 0 = -(\kappa_\mu - D_0)n_\mu - D_0(\eta_{\mu\mu}n_\mu + \eta_{\mu\bar{\mu}}\sqrt{n_\mu n_{\bar{\mu}}}\cos\phi_{\mu\bar{\mu}}) \quad (21)$$

$$\dot{\phi}_{\mu\bar{\mu}} = 0 = (\Delta_\mu - \Delta_{\bar{\mu}}) + 2D_0\left(\frac{n_\mu + n_{\bar{\mu}}}{\sqrt{n_\mu n_{\bar{\mu}}}}\right)\sin\phi_{\mu\bar{\mu}}\eta_{\mu\bar{\mu}} \quad (22)$$

where  $\eta_{\mu\alpha}$  are given by

$$\eta_{\mu\alpha} = \left( \sum_\nu \Gamma_{\mu\nu\nu\alpha}n_\nu + 2 \sum_{\nu\bar{\nu}} \sqrt{n_\nu n_{\bar{\nu}}}\cos\phi_{\nu\bar{\nu}}\Gamma_{\mu\nu\bar{\nu}\alpha} \right) (\delta_{\alpha\mu} + \delta_{\alpha\bar{\mu}}) \quad (23)$$

This set of equations by themselves constitute a complete set of equations for the steady-state phases and amplitudes of the lasing modes of the problem close to the threshold. A further simplification can be achieved by looking at the steady state condition using the natural variables  $B_{\mu\nu} = \sqrt{n_\mu n_\nu}\cos\phi_{\mu\nu}$ . Note that  $B_{\mu\mu} = n_\mu$ . The steady state condition for the phase-differences gives

$$\phi_{\mu\bar{\mu}} = 0, \pi \quad \text{or} \quad \eta_{\mu\bar{\mu}} = 0 \quad (24)$$

where for simplicity we have neglected the small splitting  $\Delta_\mu - \Delta_{\bar{\mu}}$ . The first solution  $\phi_{\mu\bar{\mu}} = 0, \pi$  is not stable, as one can see by linear stability analysis of the time-dependent equations. The second solution,  $\eta_{\mu\bar{\mu}} = 0$  is equivalent to a linear homogeneous equation for the variables  $B_{\mu\nu}$ :

$$\sum_\nu \Gamma_{\mu\nu\nu\bar{\mu}}B_{\nu\nu} + 2 \sum_{\nu\bar{\nu}} \Gamma_{\mu\nu\bar{\nu}\bar{\mu}}B_{\nu\bar{\nu}} = 0 \quad (25)$$

Imposing the steady state condition for the amplitudes,  $\dot{n}_\mu = 0$  provides a second set of inhomogeneous linear equations, similar to those in the ‘‘diagonal’’ theory discussed above.

$$\sum_\nu \Gamma_{\mu\nu\nu\mu}B_{\nu\nu} + \sum_{\nu\bar{\nu}} \Gamma_{\mu\nu\bar{\nu}\mu}B_{\nu\bar{\nu}} = 1 - \frac{\kappa_\mu}{D_0} \quad (26)$$

We will implement these equations for the circular cavity in the next section.

## 5.1. Steady State Solutions

### 5.1.1. Mode-locking in circular resonators

As already noted the cold-cavity modes of a circular resonator display exact degeneracy, hence mode-locking is an essential phenomenon which must be taken into account in order to predict the observed lasing modes. It is known within the framework of two-mode dynamics that degenerate modes lock into clock-wise or counter-clockwise propagating circular waves<sup>24</sup> with angular dependence  $e^{\pm im\phi}$ . We would like to know whether this statement is still valid when many such doublets are also interacting with other doublets. The answer is positive, as we will illustrate by considering two pairs of degenerate cold-cavity modes.

The resulting equations describe **four** modes in competition, where the modes are of the form:

$$\psi_{(1,2)}^a = J_m(nk_a r)(\cos m\phi, \sin m\phi) \quad \psi_{(1,2)}^b = J_n(nk_b r)(\cos n\phi, \sin n\phi) \quad (27)$$

where  $m \neq n$ . We furthermore have group indices (radial numbers)  $a, b$ , denoting the two groups of states.

Then, the steady state condition for the phase differences is given by

$$\dot{\phi}_{12}^a = 0 = 2D_0\left(\frac{n_1^a + n_2^a}{\sqrt{n_1^a n_2^a}}\right)\sin\phi_{12}^a\eta_{12}^a \quad (28)$$

And similarly for doublet  $b$ . Consider the coupling variables. For instance,  $\eta_{12}^a = \Gamma_{1112}^{aaaa}B_{11}^a + 2\Gamma_{1122}^{aaaa}B_{12}^a + 2\Gamma_{1122}^{abba}B_{12}^b + \Gamma_{1222}^{aaaa}B_{22}^a + \Gamma_{1112}^{abba}B_{33}^b + \Gamma_{1222}^{abba}B_{22}^b$ . Here we have defined  $\Gamma_{mnop}^{ijkl} = \int d^2x \psi_m^i(\mathbf{x})\psi_n^j(\mathbf{x})\psi_o^k(\mathbf{x})\psi_p^l(\mathbf{x})$ .

Note that for instance  $\Gamma_{1112}^{aaaa} \propto \int d\phi \cos^3 m\phi \sin m\phi = 0$ . Similarly,  $\Gamma_{1222}^{aaaa} = \Gamma_{1112}^{abba} = \Gamma_{1222}^{abba} = 0$ , because of parity, and  $\Gamma_{1122}^{abba} = 0$  because of orthogonality ( $m \neq n$ ). Thence,

$$\eta_{12}^a = \frac{2}{3} A_{aa} B_{12} \quad (29)$$

We have used the variables

$$A_{aa} = \int d^2x (\psi_1^a(\mathbf{x}))^2 (\psi_1^a(\mathbf{x}))^2, \quad A_{ab} = \int d^2x (\psi_{1,2}^a(\mathbf{x}))^2 (\psi_{1,2}^b(\mathbf{x}))^2, \quad A_{bb} = \int d^2x (\psi_1^b(\mathbf{x}))^2 (\psi_1^b(\mathbf{x}))^2 \quad (30)$$

Then,  $\Gamma_{1122}^{aaaa} = \frac{1}{3} A_{aa}$  and  $\Gamma_{1122}^{bbbb} = \frac{1}{3} A_{bb}$ . There are two possible distinct stationary solutions:  $\sin \phi_{12} = 0$  or  $\eta_{12} = 0$ .

For the case of  $\sin \phi_{12} = 0$ , i.e.  $\phi_{12} = 0, \pi$ , we obtain

$$\frac{1}{2} \dot{B}_{11}^a = -(\kappa_1^a - D_0) B_{11}^a - D_0 \left( \eta_{11}^a B_{11}^a + \frac{2}{3} A_{aa} B_{12}^a B_{12}^a \right) \quad (31)$$

Symmetry considerations give  $\eta_{11}^a = A_{aa} B_{11}^a + \frac{1}{3} A_{aa} B_{22}^a + A_{ab} (B_{11}^b + B_{22}^b)$ . Noting that  $(B_{12}^a)^2 = B_{11}^a B_{22}^a \cos^2 \phi_{12}$ , we end up again with a linear equation for  $B_{ij}^a$ . Similar considerations apply to the modes of the  $b$ -doublet. Noting that the equations are symmetric with respect to  $B_{11}^a \leftrightarrow B_{22}^a$  and  $B_{11}^b \leftrightarrow B_{22}^b$ , defining  $n_a = B_{11}^a = B_{22}^a$  and  $n_b = B_{11}^b = B_{22}^b$ , we obtain

$$\left(1 - \frac{\kappa_a}{D_0}\right) = 2A_{aa}n_a + 2A_{ab}n_b \quad (32)$$

$$\left(1 - \frac{\kappa_b}{D_0}\right) = 2A_{bb}n_b + 2A_{ab}n_a \quad (33)$$

This is the ‘‘off-diagonal’’ version of the linear steady state equations that we have been using (Eq. (14)). Note that this solution corresponds to  $\phi_{12} = \phi_{34} = 0, \pi$ . As already noted, it can be shown that this solution is unstable by considering the linear stability analysis of the time-dependent near-threshold equations.

The case  $\eta_{12} = 0$  is equivalent to  $\cos \phi_{12} = 0$ , so that  $\phi_{12} = \pm \frac{\pi}{2}$ . The steady state equations are then

$$\left(1 - \frac{\kappa_a}{D_0}\right) = \frac{4}{3} A_{aa} n_a + 2A_{ab} n_b \quad (34)$$

$$\left(1 - \frac{\kappa_b}{D_0}\right) = \frac{4}{3} A_{bb} n_b + 2A_{ab} n_a \quad (35)$$

Again, through a linear stability analysis it is possible to show that this is the stable branch. As can be seen, each degenerate set of modes lock into a clockwise or counter-clockwise rotating wave. Let us note here the connection to the generalized free-energy approach<sup>25</sup>: A modal distribution which has the largest modal volume burns the inversion most efficiently and minimizes a particular action integral. The mode volume is maximized for the case with  $\phi_{12} = \pm \frac{\pi}{2}$ , corresponding to a uniform running wave  $e^{\pm im\phi}$ . This justifies our use of modes with angular dependence  $e^{\pm im\phi}$  in Section 3.1.

### 5.1.2. Mode-locking in deformed resonators

The situation for deformed resonators is complicated by the fact that exact degeneracies cease to exist once the cavity shape is deformed smoothly from a rotationally symmetric shape. However, for shapes which are invariant under discrete point symmetries, near-degeneracies are typical. Specifically, it is known that the subset of modes based on stable periodic orbits form quasi-multiplets, and that the multiplicity and symmetry properties of stable-orbit quasi-multiplets are intimately connected to the symmetry and multiplicity of the underlying periodic orbits.<sup>20</sup> The *average* quasi-multiplet splitting scales as  $\delta \sim e^{-\mathcal{A}kR}$ , where  $\mathcal{A}$  is the phase space area occupied by the corresponding stable island.<sup>20, 26</sup> Under such circumstances, a multi-frequency solution can exist if we assume  $\Delta \gg \gamma_{\parallel} \gg \delta$ , where  $\Delta$  is the typical mean level spacing. In that case, as can be seen from Eq. (3), the beating terms in  $D(\mathbf{x}, t)$  will be down by  $\gamma_{\parallel}/\Delta$  with respect to the stationary part, while multiplets

are expected to lock to a common lasing frequency contributing to the latter. Thus, there will be a “diagonal” and an “off-diagonal” contribution to the stationary inversion  $D(\mathbf{x})$ , as in Eq. (20). The validity of this scenario of course is complicated by the presence of modes based on the chaotic portion of the phase space, which also interact with stable orbit modes; further study is required to evaluate the effect of these interactions on the mode-locking scenarios.

Here however, we will treat only a single pair of such modes in connection with the experiments of Gmachl et al.<sup>6</sup> As noted above, based on evidence from spectral measurements and farfield distributions, the lasing modes at high deformations were identified to be second order transverse modes corresponding to the stable periodic orbit with the shape of a bowtie<sup>6,27</sup> (See Fig. 6). In Fig. 12) we display the time dynamics of such a bow-tie doublet. We find that the frequency locks about a certain pump strength as expected; the critical value of the pumping depends strongly on  $\Delta$ , the cold-cavity frequency difference of the modes in question. In addition, the field intensities and phases approach steady-state values which are equal to those found from the steady-state method used to produce all the results above. Mode-locking can lead to output patterns which are different from those of any single cold-cavity mode and even violate the discrete symmetries of the resonator.<sup>16</sup> It has already been shown<sup>27</sup> that the experimental emission patterns of Gmachl et al.<sup>6</sup> are better fit by superposing cold-cavity doublet emission patterns as would result from mode-locking. We will present a complete theoretical analysis of the mode-locked emission from several bow-tie modes elsewhere.<sup>28</sup>

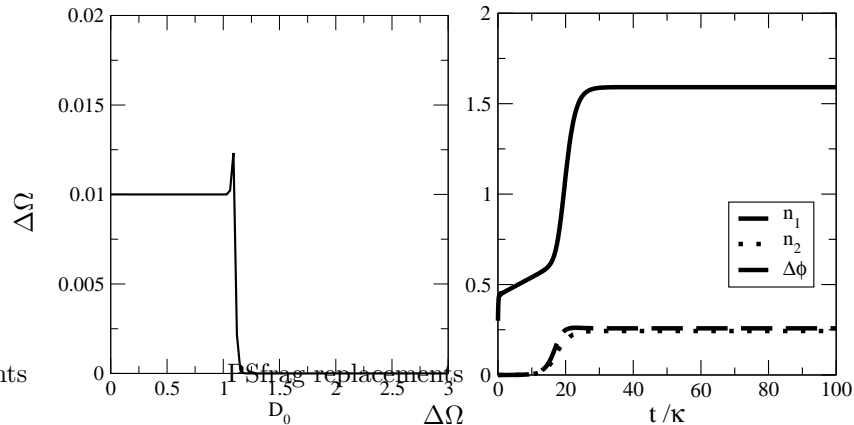


**Figure 12.** (a) The variation with pump strength  $D_0$  of the difference in lasing frequencies  $\Delta\Omega = \Omega_1 - \Omega_2$  of the two modes corresponding to a bow-tie doublet. Note that frequency-locking takes place above a critical value of the pump strength  $D_c \approx 1.1$ . (b) Time-dynamics of two-mode lasing for quasi-degenerate second order bowtie modes above the mode-locking threshold. The two mode intensities grow to equal steady-state values and their phase difference locks at  $\Delta\phi = \pi/2$  as predicted by the analysis above. at  $nkR \approx 122.7$ . The parameters chosen are  $\gamma_{\parallel} = 10$ ,  $\kappa_1 = 1.0$ ,  $\kappa_2 = 1.02$ ,  $D_0 = 1.5$  and  $\Delta = 0.01$ ; all parameters are scaled with respect to the cavity decay rate of one of the modes.

## ACKNOWLEDGMENTS

We acknowledge helpful discussions with Takahisa Harayama, Claire Gmachl and Harald Schwefel. This work was supported by NSF grant DMR-0408638.

## REFERENCES

1. R. K. Chang and A. K. Campillo, eds., *Optical Processes in Microcavities*, World Scientific, Singapore, 1996.
2. Y. Yamamoto and R. E. Slusher, “Optical processes in microcavities,” *Phys. Today* **46**, pp. 66–73, 1993.
3. K. J. Vahala, “Optical microcavities,” *Nature* **424**, pp. 839–846, 2003.
4. J. U. Nöckel, A. D. Stone, and R. K. Chang, “ $q$ -spoiling and directionality in deformed ring cavities,” *Opt. Lett.* **19**, pp. 1693–1695, 1994.
5. J. U. Nöckel and A. D. Stone, “Ray and wave chaos in asymmetric resonant optical cavities,” *Nature* **385**, pp. 45–47, 1997.

6. C. Gmachl, F. Capasso, E. E. Narimanov, J. U. Nöckel, A. D. Stone, J. Faist, D. L. Sivco, and A. Y. Cho, "High-power directional emission from microlasers with chaotic resonators," *Science* **280**, pp. 1556–1564, 1998.
7. H. G. L. Schwefel, H. E. Tureci, A. D. Stone, and R. K. Chang, "Progress in asymmetric resonant cavities: Using shape as a design parameter in dielectric microcavity lasers," in *Optical Processes*, K. J. Vahala, ed., World Scientific, 2004.
8. H. G. L. Schwefel, N. B. Rex, H. E. Tureci, R. K. Chang, A. D. Stone, T. Ben-Messaoud, and J. Zyss, "Dramatic shape sensitivity of directional emission patterns from similarly deformed cylindrical polymer lasers," *J. Opt. Soc. Am. B* **21**, pp. 923–934, 2004.
9. N. B. Rex, H. E. Tureci, H. G. L. Schwefel, R. K. Chang, and A. D. Stone, "Fresnel filtering in lasing emission from scarred modes of wave-chaotic optical resonators," *Phys. Rev. Lett.* **88**, p. art. no. 094102, 2002.
10. C. Gmachl, E. E. Narimanov, F. Capasso, J. N. Baillargeon, and A. Y. Cho, "Kolmogorov-Arnold-Moser transition and laser action on scar modes in semiconductor diode lasers with deformed resonators," *Opt. Lett.* **27**, pp. 824–826, 2002.
11. N. B. Rex, *Regular and chaotic orbit Gallium Nitride microcavity lasers*. PhD thesis, Yale University, New Haven, USA, 2001.
12. H. Haken, *Light (Volume 2)*, North-Holland Physics Publishing, Amsterdam, Netherlands, 1985.
13. M. S. III, M. O. Scully, and W. E. L. Jr., *Laser Physics*, Addison-Wesley, Massachusetts, USA, 1974.
14. H. Haken and H. Sauermann, "Nonlinear interactions of laser modes," *Z. Phys.* **173**, p. 261, 1963.
15. T. Harayama, P. Davis, and K. S. Ikeda, "Whispering gallery mode lasers," *Progress Of Theoretical Physics Supplement*, pp. 363–374, 2000.
16. T. Harayama, T. Fukushima, S. Sunada, and K. S. Ikeda, "Asymmetric stationary lasing patterns in 2d symmetric microcavities," *Physical Review Letters* **91**, 2003.
17. T. Harayama, P. Davis, and K. S. Ikeda, "Stable oscillations of a spatially chaotic wave function in a microstadium laser," *Physical Review Letters* **90**, 2003.
18. F. T. Arecchi, G. L. Lippi, G. P. Puccioni, and J. R. Tredicce, "Deterministic chaos in laser with injected signal," *Opt. Commun.* **51**, pp. 308–314, 1984.
19. H. Fu and H. Haken, "Multifrequency operations in a short-cavity standing-wave laser," *Physical Review A* **43**, pp. 2446–2454, 1991.
20. H. E. Tureci, H. G. L. Schwefel, A. D. Stone, and E. E. Narimanov, "Gaussian-optical approach to stable periodic orbit resonances of partially chaotic dielectric micro-cavities," *Opt. Express* **10**, pp. 752–776, 2002.
21. T. Harayama, P. Davis, and K. S. Ikeda, "Nonlinear whispering gallery modes," *Physical Review Letters* **82**, pp. 3803–3806, 1999.
22. J. U. Nöckel, *Resonances in nonintegrable open systems*. PhD thesis, Yale University, New Haven, USA, 1997.
23. T. S. Misirpashaev and C. W. J. Beenakker, "Lasing threshold and mode competition in chaotic cavities," *Phys. Rev. A* **57**, pp. 2041–2045, 1998.
24. L. A. Lugiato, F. Prati, L. M. Narducci, and G. L. Oppo, "Spontaneous breaking of the cylindrical symmetry in lasers," *Optics Communications* **69**, pp. 387–392, 1989.
25. M. Brambilla, L. A. Lugiato, V. Penna, F. Prati, C. Tamm, and C. O. Weiss, "Transverse laser patterns .2. variational principle for pattern selection, spatial multistability, and laser hydrodynamics," *Physical Review A* **43**, pp. 5114–5120, 1991.
26. V. A. Podolskiy and E. E. Narimanov, "Semiclassical description of chaos-assisted tunneling," *Physical Review Letters* **91**, 2003.
27. H. E. Tureci, H. G. L. Schwefel, P. Jacquod, and A. D. Stone, "Modes of wave-chaotic dielectric resonators," *Progress In Optics* **47**, 2005.
28. H. E. Tureci and A. D. Stone unpublished.